Front. Environ. Sci. Eng. 2024, 18(4): 44
https://doi.org/10.1007/s11783-024-1804-7

RESEARCH ARTICLE

Enhanced Fenton-like process over Cu/L(+)-ascorbic acid co-doping mesoporous silica for toxicity reduction of emerging contaminants

Yuhang Liu, Wenxuan Deng, Xiaojun Wu, Chun Hu, Lai Lyu (✉)

Key Laboratory for Water Quality and Conservation of the Pearl River Delta (Ministry of Education), Institute of Environmental Research at Greater Bay, Guangzhou University, Guangzhou 510006, China

HIGHLIGHTS

- Cu-C-MSNs are developed via a co-doping step of Cu with L(+)-ascorbic acid.
- Cu-C-MSNs show superb performance in removing contaminants and purifying wastewater.
- The performance is owing to the polarization electric field and cation-π structures.
- The biological toxicity of bisphenol A is considerably weakened after the reaction.

GRAPHIC ABSTRACT

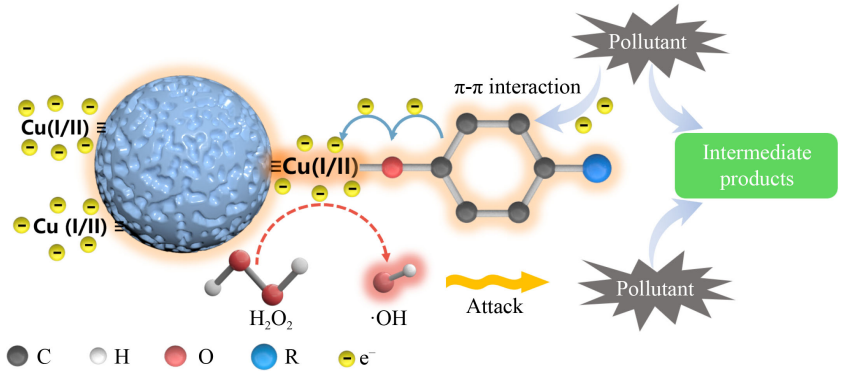

ARTICLE INFO

Article history:
Received 26 July 2023
Revised 14 November 2023
Accepted 15 November 2023
Available online 15 December 2023

Keywords:
Cation-π structures
Polarization electric field
Fenton-like process
Contaminants cleavage

ABSTRACT

Effective removal of emerging contaminants (ECs) to minimize their impacts on human health and the natural environment is a global priority. For the removal of ECs in water, we fabricated a seaweed spherical microsphere catalyst with Cu cation-π structures by *in situ* doping of Cu species and ascorbic acid in mesoporous silica (Cu-C-MSNs) via a hydrothermal method. The results indicate that bisphenol A (BPA) is substantially degraded within 5 min under natural conditions, with its biological toxicity considerably weakened. Moreover, industrial wastewater could also be effectively purified by Cu-C-MSNs/H_2O_2 system. The presence of metal sites and the complexation of ECs via cation-π interaction and π-π stacking on the catalyst surface were directly responsible for the polarization distribution of electrons, thus activating H_2O_2 and dissolved oxygen (DO). The removal of contaminants could be attributed primarily to 1) the activation of H_2O_2 into $^{\bullet}OH$ to attack the contaminants and 2) self-cleavage because of the transfer of electrons from the contaminants to the catalysts. This study provides an innovative solution for the effective treatment of ECs and has positive implications for easing global environmental crises.

1 Introduction

Water pollution is a serious global environmental issue (Taheran et al., 2018; Alimba and Faggio, 2019; Rathi et al., 2021; Tang et al., 2021; Morin-Crini et al., 2022), exacerbated by the diffusion of emerging contaminants (ECs), including endocrine disruptors (EDs), persistent organic pollutants (POPs), and antibiotics, in aquatic environment worsens this global problem and has adversely affected the ecosystem and human health (Sauvé and Desrosiers, 2014; Khan et al., 2022; Wang and Yu, 2022). Bisphenol A (BPA), a plastic precursor used in synthesizing polycarbonate and epoxy resin, is a typical ED detected in diverse aquatic environments

✉ Corresponding author
E-mail: lyulai@gzhu.edu.cn

(Almeida et al., 2018; Trivedi and Chhaya, 2022; Wang et al., 2022a; Xing et al., 2022a). Epidemiological surveys and animal experiments have shown that BPA exposure damages multiple organ systems, including reproductive, neurological, immune, and endocrine systems (Hines et al., 2018; Xiao et al., 2020; vom Saal and Vandenberg, 2021). Despite consuming considerable energy and chemicals, conventional water treatment technologies face challenges in effectively degrading these ECs owing to their structural stability (Tran and Gin, 2017; Khan et al., 2021). This necessitates the urgent development of low-energy-consuming and highly efficient water treatment technologies to ensure rapid degradation and toxicity reduction of ECs.

Advanced oxidation processes (AOPs) are considered effective degradation technologies for organic pollutants in water because of the benefits from the aggressive nature of the generated reactive oxygen species such as hydroxyl radicals (•OH), superoxide radicals ($O_2^{\bullet-}$), and singlet oxygen ($^1O_2$) (Tran and Gin, 2017; Cuerda-Correa et al., 2019; Giwa et al., 2021). However, despite using extensive input of oxidants and driving forces such as light, electricity, and ultrasound, these technologies require high-energy inputs to remove stubborn ECs (Do Minh et al., 2020; Scaria et al., 2021). Fenton reaction is a widely used technique of AOPs (Yazici Guvenc and Varank, 2021). The •OH produced by the reaction of Fe^{2+} and H_2O_2 rapidly attacks the organic pollutants (Gao et al., 2022). However, this reaction faces considerable limitations, including a restricted acidity range (pH 2–3), extensive consumption of unrecyclable iron salts, and the generation of hazardous iron sludge (Yamaguchi et al., 2018; Gao et al., 2022). Although heterogeneous Fenton/Fenton-like reactions have partially alleviated these problems (Zhao et al., 2022), the huge energy consumption continues to be an inevitable challenge owing to the identical reaction principles (Lu et al., 2020). In particular, the invalid decomposition of H_2O_2 commonly overcomes the rate limitation of high-valence metal reduction. In these systems, H_2O_2 molecules act as electron acceptors and are reduced to •OH through O–O bond cleavage. Simultaneously, they act as electron donors and are oxidized to $O_2^{\bullet-}$ or the ineffectual O_2 via O–H bond breakage. Consequently, the H_2O_2 consumption exceeds the theoretical value by 100 times in certain systems (Lyu and Hu, 2017). Altering the degradation process of contaminants and the decomposition path of H_2O_2 is essential for reducing H_2O_2 consumption and realizing a low-consumption Fenton-like water treatment technology.

Previously, we had found that ECs possess a large number of electrons and chemical energy (Lyu et al., 2015b; 2016a; 2016b), which can be utilized to reduce oxidizing substances in wastewater via the construction of dual-reaction centers (DRCs) with electron-poor/-rich micro-areas and driving effect of the non-equilibrium potential difference on the catalyst surface (Lyu et al., 2020; Zhang et al., 2020b; Cao et al., 2021; Gao et al., 2021). Thus, ECs can be eliminated rapidly via synergistic interactions from surface cleavage and free radical attack, and the consumption of peroxide reduces substantially. These studies inspire us that pollutant energy can be utilized to purify wastewater, thereby saving energy. However, this strategy still faces a significant scientific challenge as the EC structures are stable making it difficult to activate the internal energy and electrons. Cation–π interactions are key intermolecular binding forces between cations and electron-rich π orbitals, which can drive the electron transfers of the types of π→cation (σ donation) and cation→π* (π back-donation) (Gebbie et al., 2017; Lyu et al., 2017; Wang et al., 2021b). Thus, the activation of stable ECs by cation-π structures formed by metal-organic complexation becomes feasible. Furthermore, interfacial confinement fundamentally alters the energetics of cation–π-mediated assembly. These fundamental findings on cation-π interactions hold promise for the development of pollutant-energy-driven low-consumption water treatment technologies, which remains a global challenge in the field of environmental remediation.

Herein, to overcome this challenge, a novel catalyst (Cu-C-MSNs), with Cu cation-π structures was prepared by surface modification of SiO_2 porous microspheres via a co-doping step of L(+)-ascorbic acid with Cu species. Cu-C-MSNs, used to degrade ECs in combination with H_2O_2 as Fenton-like catalysts, exhibited excellent performance. The degradation rate of BPA exceeded 85% within 5 min and was accompanied by a significant reduction in toxicity. Cu-C-MSNs were also resistant to the interference of natural organic matter (NOM) and various types of salts while achieving satisfactory purification effects on actual wastewater samples from printing and dyeing. The formation of C–O–Cu bonds (cation–π structures) and the complexation of ECs through cation-π interaction and π-π stacking on the catalyst surface were found crucial for the activation and utilization of the electrons in the ECs; this ensured reduced consumption of energy during the reaction and efficient water purification. A corresponding interface reaction mechanism involving ECs degradation was also proposed in this study based on a series of experiments.

2 Experimental section

2.1 Materials

Bisphenol A (BPA, ⩾ 98%, Adamas, China), phenytoin (PHT, ⩾ 98%, Adamas, China), diphenhydramine (DP, ⩾ 98%, Adamas, China), tetracycline (TC, ⩾ 98%, Titan, China), 5,5-dimethyl-pyrroline *N*-oxide (DMPO, 99%, Dojindo, Japan), *N*, *N*-diethyl-p-phenylenediamine

sulfate (DPD, 98%, Adamas, China), copper nitrate hydrate ($Cu(NO_3)_2 \cdot 3H_2O$, ≥ 99%, Titan, China), L(+)-Ascorbic acid (≥ 99%, Titan, China), ammonium hydroxide solution (25%–28%, Titan, China), hexadecyl trimethyl ammonium bromide (CTAB, 99%, Titan, China), hydrogen peroxide (H_2O_2, 30%, w/w, Guangzhou Brand, China), horseradish peroxidase (POD, Adamas, China), tetraethyl orthosilicate (TEOS, 99%, Titan, China). All of the above reagents can be used without further purification.

2.2 Synthesis of Cu-C-MSNs

Cu-C-MSNs were synthesized using an enhanced hydrothermal process. Briefly, 0.12 g $Cu(NO_3)_2 \cdot 3H_2O$ and 0.05 g L(+)-ascorbic acid were dissolved in 50 mL deionized water, which was stirred using a mechanical stirrer, followed by stirring into a homogeneous phase. Similarly, hexadecyl trimethyl ammonium bromide (CTAB) was dispersed in anhydrous ethanol (70 mL) and stirred into another homogeneous phase. The two samples were mixed and stirred at 25 °C for 45 min to which 8 mL tetraethyl orthosilicate (TEOS) and ammonium hydroxide were added dropwise to form a colloidal solution. The resulting mixture was then placed in a Teflonlined steel autoclave and heated to 110 °C for 24 h. The mixture was cooled naturally, and the product was filtered and washed several times. Finally, the sample was placed in an oven at 60 °C for 12 h and calcined in a muffle furnace at 550 °C for 6 h to obtain Cu-C-MSNs. The reference standards SiO_2 NSs and Cu-MSNs were prepared using the same procedure.

2.3 Characterization

The surface morphology and elemental composition of the catalysts were obtained by a scanning electron microscope (Hitachi Regulus8100, Hitachi, Japan) and a transmission electron microscope (FEI Talos F200X, Thermo Fisher, USA). The crystallinity of the catalysts was characterized by Philips X'Pert PRO SUPER diffractometer (XRD, Philips, China). The functional groups on the catalyst surface were detected by a Bruker Vertex 70 FTIR spectrometer (Bruker, USA). X-ray photoelectron spectroscopy (XPS) (PHI-5000versaprobeIII, ULVAC-PHI, China) was used to collect elemental information on the catalyst surface. An electron paramagnetic resonance spectrometer (EPRS, Bruker, USA) model Bruker A300-10/12 was used for the detection of reactive oxygen species. The concentration of metal ions in the solution was detected by ICP-OES (PerkinElmer Optima 5300 DV, PerkinElmer, USA) to the stability of the catalysts.

2.4 Procedures and analysis

The endocrine disruptor bisphenol A (BPA), the drug phenytoin (PHT), diphenhydramine (DP), tetracycline (TC), and the synthetic dye rhodamine B (RhB) were selected as target contaminants to evaluate the performance of the catalyst due to the biodegradability and other potential toxicity of these materials. According to the optimum activity of bisphenol A degradation obtained by experiments, the optimum concentration of catalyst and H_2O_2 is 1.0 g/L and 0.01 mol/L. In the basic reaction experiment, under the condition of neutral pH value, the catalyst powder (0.05 g) was evenly dispersed into 50 mL contaminants aqueous solution by magnetic rotor and thermostat water bath, and the temperature of the thermostat water bath was set to 35 °C. After the adsorption/desorption equilibrium between the catalyst and the contaminants was reached, 0.01 mol/L of H_2O_2 was added to the solution by drop. Samples were taken at certain time points using a 1 mL sampler and filtered through a Millipore filter for subsequent analysis. The contaminants concentrations were measured by high-performance liquid chromatography (HPLC). The details of other procedures and analyses are given in the Supplementary material.

3 Results and discussion

3.1 Structural characterization

A catalyst with seaweed spherical structures (Cu-C-MSNs) was developed by doping mesoporous silica with Cu species and ascorbic acid via an enhanced hydrothermal reaction. Figure 1(a) shows the steps to prepare the Cu-C-MSNs. $Cu(NO_3)_2 \cdot 3H_2O$ and ascorbic acid with a mass ratio of 1.5:1 were dispersed in deionized water and mixed with an ethanol solution containing 0.004 mol CTAB. Subsequently, TEOS and ammonium hydroxide were added in 1:1 ratio and stirred for 2 h. The mixture was transferred to a Teflonlined autoclave for the hydrothermal reaction at 110 °C. Thereafter, the samples were thoroughly washed several times and dried. Finally, the obtained solid was calcined in air to form Cu-C-MSNs.

The scanning electron microscopy (SEM) images (Figs. 1(b) and 1(c)) illustrate that the Cu-C-MSNs are seaweed spherical structures with a narrow size distribution range. The crystalline copper species were not observed in the transmission electron microscopy (TEM) images (Figs. 1(d) and 1(e)) and the Cu-C-MSNs showed a porous structure, suggesting the absence of copper oxide cluster formation and the incorporation of copper into the silica framework. The elemental mappings of the Cu-C-MSNs (Fig. 1(f)) indicated good dispersion of O, Si, Cu, and C.

According to the powder X-ray diffraction (XRD) in Fig. 2(a), the peaks at $2\theta = 23°$ for Cu-C-MSNs and C-SiO_2 corresponded to amorphous silica, whereas no peaks attributed to Cu oxides, indicating that the introduced Cu species were indeed dispersed into the SiO_2 framework

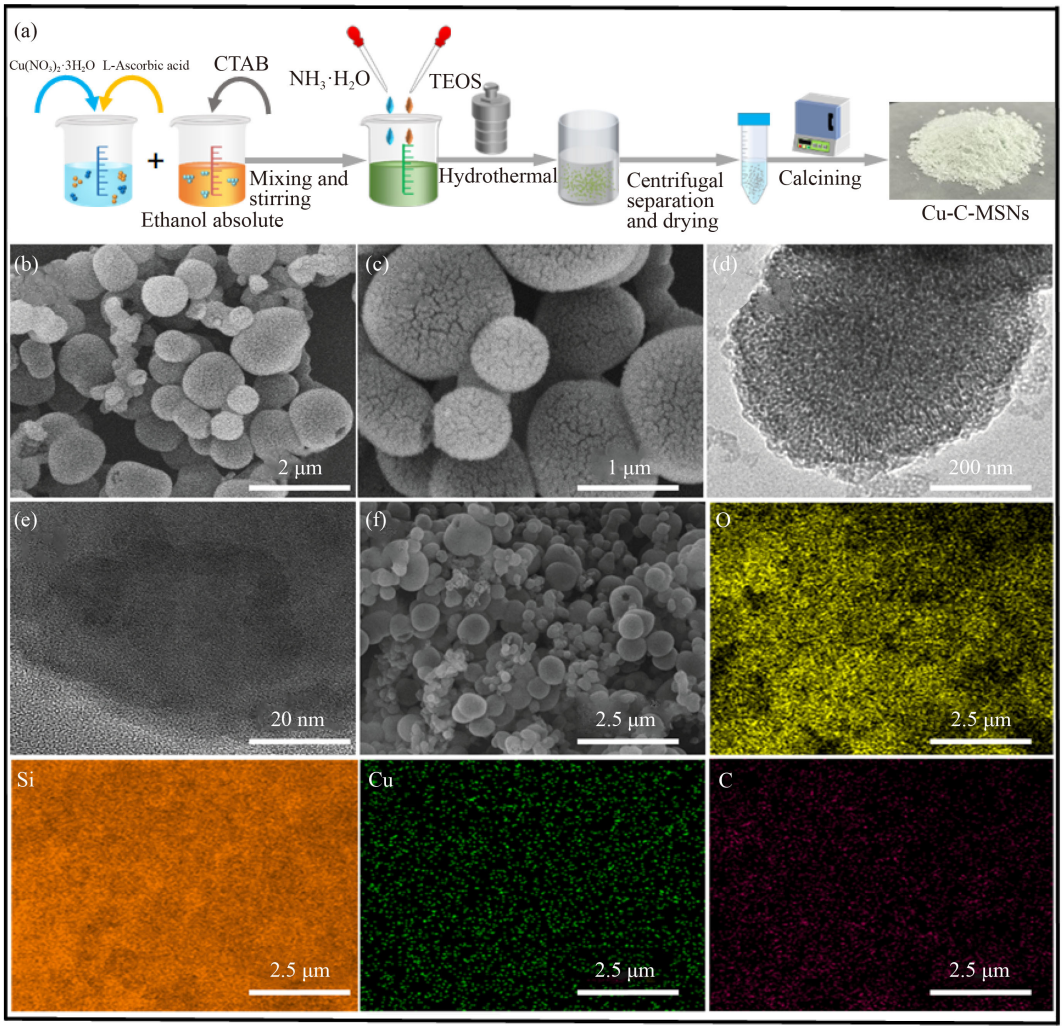

Fig. 1 (a) Preparation process of Cu-C-MSNs. (b) and (c) SEM images of Cu-C-MSNs. (d) and (e) TEM images of Cu-C-MSNs. (f) Element mapping of O, Si, Cu and C from SEM images.

(Lyu et al., 2015a). Figure 2(b) presents the FT-IR spectra of the prepared samples, providing more information about the chemical bonds and groups. The two characteristic peaks at 3450.0 and 1635.3 cm^{-1} were attributed to the stretching vibration of the -OH group on the SiO_2 surface [v(OH)] and C=O, respectively (Wang et al., 2022b). The addition of copper species shifted these two peaks to lower wave numbers (3430.7 and 1633.4 cm^{-1}), indicating that the hydroxyl groups on the catalyst surface contacted with the copper species, and C=O bonds were converted to C–O–Cu bonds. After absorbing BPA for 30 min, C–O–Cu bonds were red-shifted to 1631.4 cm^{-1} owing to the complexation of copper species and the benzene rings of BPA to form new Cu–O–C bonds (cation-π structures). The peak at 1095.0 cm^{-1} indicates Si–O–Si asymmetric stretching vibration, and the peaks at 804.2 and 466.7 cm^{-1} represent the Si–O symmetric stretching vibrations. The peak located at 804.2 cm^{-1} where the Si–O–Cu bonds were formed on the surface shifted to 806.1 cm^{-1} after Cu doping. Similarly, the peaks at 806.1 and 466.7 cm^{-1} moved to 802.2 and 470.6 cm^{-1}, respectively, after absorbing BPA for 30 min, which could be attributed to the deprotonation of phenolic hydroxyl groups in BPA or intermediates of BPA and the microenvironment changing of the first coordination layer of copper (Mitić et al., 2009). These results suggest the complexation of BPA on copper species by bonding with the oxygen atoms in the phenolic hydroxyl group.

X-ray photoelectron spectroscopy (XPS) was performed to further analyze and validate the above phenomena. The binding energy peaks of Cu $2p_{3/2}$ at 932.48 and 934.68 eV were attributed to Cu(I) and Cu (II) (Fig. 2(c)) (Xing et al., 2022b). The appearance of a satellite peak at 943.9 eV confirmed the existence of Cu (II) (López-Suárez et al., 2009). The binding energies of Cu(I) and Cu(II) decreased by 0.02 eV and increased by 0.12 eV compared to those of Cu_2O (932.5 eV) and CuO (933.6 eV), which was attributed to the conversion of parts of Cu(II) to Cu(I) (electron-rich centers) by acquiring excess electrons during the synthesis.

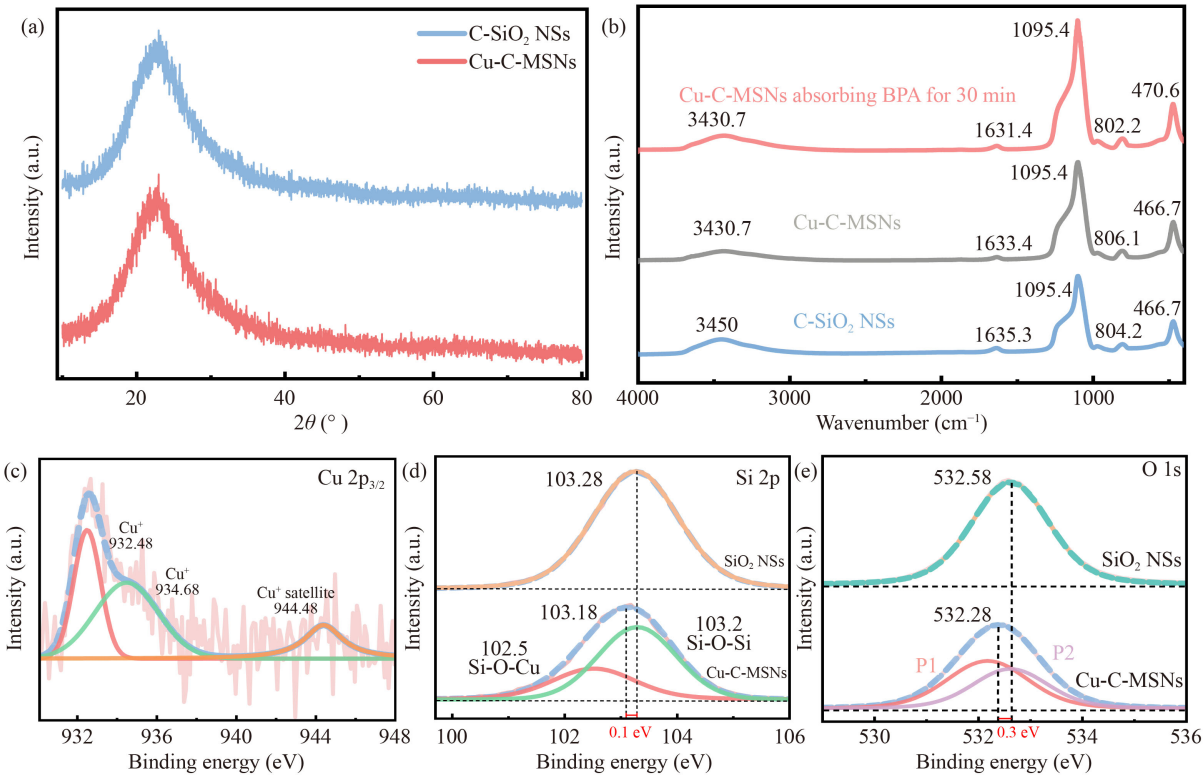

Fig. 2 (a) XRD patterns of C-SiO_2 NSs and Cu-C-MSNs. (b) FT-IR spectra of Cu-C-MSNs. XPS orbit spectrum of Cu-C-MSNs and SiO_2 NSs in (c) Cu $2p_{3/2}$, (d) Si 2p, (e) O 1s.

Compared with copper, the higher electron affinity of silicon leads to the transfer of electrons from copper to silico (Zhang et al., 2012). This resulted in a higher Cu $2p_{3/2}$ binding energy for Cu(II), which further confirmed the formation of Si–O–Cu in the sample (Lyu et al., 2015a). Cu (II) was converted to Cu (I) as a result of L(+)-ascorbic acid reduction, which was beneficial to contaminant degradation. Fig. 2(d) shows a typical Si-O-Si of Cu-C-MSNs and SiO_2 NSs (Bing et al., 2017). Doping Cu species caused a decrease in the Si 2p binding energy as Si was substituted by Cu to form Cu-O-Si, which implied an increase of the electron cloud density around the Si atoms. Figure 2(e) shows the O 1s orbital of SiO_2 NSs and Cu-C-MSNs. The O 1s peak (532.58 eV) of the SiO_2 NSs was attributed to absorbed oxygen, including those in the hydroxyl, carboxyl, or other oxygen-containing groups (Zhang et al., 2020a). The introduction of Cu led to a skewing of O 1s toward lower binding energies. According to the split-peak fitting results, P1 at 532.18 eV and P2 at 532.68 eV correspond to lattice and surface oxygen, respectively. The above evidence indicates that electrons gather around the O atoms via Si–O–Cu (lattice oxygen) after Si is substituted with Cu. The binding energy of C 1s orbit (Fig. S1) of Cu-C-MSNs was increased, which is attributed to the formation of C–O–Cu bonds (cation-π structures). These characterization results show the successful formation of a polarization electric field on the Cu-C-MSN surface, which may be crucial for its excellent performance in Fenton-like reactions.

3.2 Catalytic performance for ECs removal

The activity of Cu-C-MSNs was evaluated via the degradation of ECs, including the endocrine disruptor BPA, carcinogenic dye rhodamine B (RhB), antihistamine drug diphenhydramine (DP), carcinogenic drug phenytoin (PHT), and antibiotic tetracycline (TC) under natural conditions. In Fig. 3(a), only 20.0% and 32.11% of BPA were removed in C-SiO_2 NSs/H_2O_2 and Cu-MSNs/H_2O_2 systems, respectively. Surprisingly, in Cu-C-MSNs/H_2O_2 system, 87% BPA was removed within 5 min and nearly 100% was removed in 2 h. This effect was induced by the unbalanced distribution of electrons on the catalyst surface and the attack by ROS. Different typical ECs were also effectively removed similarly by Cu-C-MSNs/H_2O_2 system Fig. 3(b). The maximum removal rates of RhB and DP were 85.4% and 80.0%, respectively, in two hours. Compared to Cu-C-MSNs/H_2O_2 system, the consumption of H_2O_2 in Cu-C-MSNs/H_2O_2/BPA system was only 35% (Fig. S2), indicating Cu-C-MSNs is an efficient, low-consumption catalyst for wastewater purification.

The ion leaching rate and recycling performance were

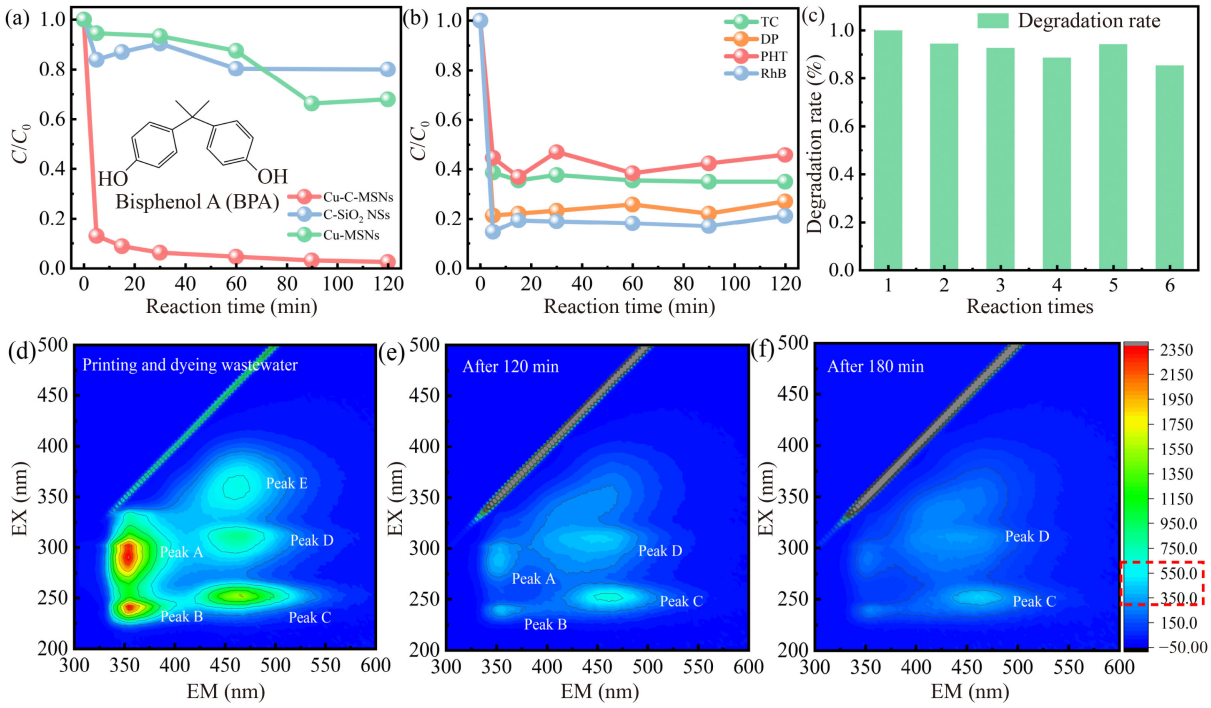

Fig. 3 (a) Degradation of BPA in the Cu-C-MSNs, C-SiO_2, Cu-MSNs system with H_2O_2. (b) The catalytic effect of different contaminants. (c) Reusability of Cu-C-MSNs for BPA degradation. (d) Excitation-Emission-Matrix Spectra of printing and dyeing wastewater. (e) Wastewater after 120 min of degradation of Cu-C-MSNs/H_2O_2 system. (f) Wastewater after 180 min of degradation of Cu-C-MSNs/H_2O_2 system. Reaction conditions: [catalyst] = 1.0 g/L, [H_2O_2] = 0.01 mol/L, [BPA] =0.01 g/L, t = 35 °C.

evaluated to determine the stability of the Cu-C-MSNs. The concentration of Cu ions in the solution after the reaction was in the range of 0.05–0.1 mg/L, well below the limits prescribed by United States regulations. The solid catalyst was recovered through filtration, washing, and drying during the recycling performance test for cycle experiments (Fig. 3(c)). There was no significant decrease in the performance of Cu-C-MSNs after six successive cycles of degradation, and the contaminants removal was stabilized at 85.5%. Thus, Cu-C-MSN was verified to be an effective and reliable heterogeneous Fenton catalyst with potential for practical applications. Printing and dyeing wastewater from an industrial park was used to investigate the performance of the catalyst. In Fig. 3(d), two strong peaks were detected at λEX/λEM = 290/353 nm (Peak A) and λEX/λEM = 241/354 nm (Peak B), representing dissolved microbial metabolites and contaminant molecules in the untreated sample, respectively. The region centered at λEX/λEM = 252/463 nm (Peak C), λEX/λEM = 310/460 nm (Peak D), and λEX/λEM = 360/460 nm (Peak E) represent dissolved organic matters (DOM), including fulvic acids and humic acids (HA) (He et al., 2013; Zhang et al., 2015; Wang et al., 2021a). In Figs. 3(e) and 3(f), the intensity of peak A was significantly reduced after the reaction in Cu-C-MSNs/H_2O_2 system, indicating the purification of printing and dyeing wastewater. The refractory dye molecules were preferentially removed from wastewater during the reaction, thus ensuring rapid and efficient purification. The rapid degradation of contaminants may be attributed to the cation-π interaction and polar complexation between the catalyst, contaminants, and DOM, improving the electron transfer efficiency among these three substances.

3.3 Impact of environmental factors for Cu-C-MSNs/H_2O_2 system

The impact of environmental factors, including the initial pH, effect of different anions, catalyst, H_2O_2 concentration, contaminants concentration, and HA concentrations, on the degradation by Cu-C-MSNs/H_2O_2 system was investigated.

In Fig. 4(a), contaminant degradation was enhanced by increasing the catalyst concentration from 0.1 to 1.0 g/L. Once the catalyst concentration exceeded 1.0 g/L, the performance was weakened, which may be due to a reduction in the interfacial electron transfer efficiency by the agglomeration of catalyst particles. Thus, the optimum catalyst concentration was 1.0 g/L. The activity of the Cu-C-MSN system was enhanced with increasing H_2O_2 concentrations, implying that excessive H_2O_2 increased the supply of $^{\bullet}$OH to attack the contaminants. Considering the economic cost and benefit, the optimal initial H_2O_2 concentration was found to be 0.01 mol/L (Fig. 4(b)). In Fig. 4(c), the activity of the catalyst

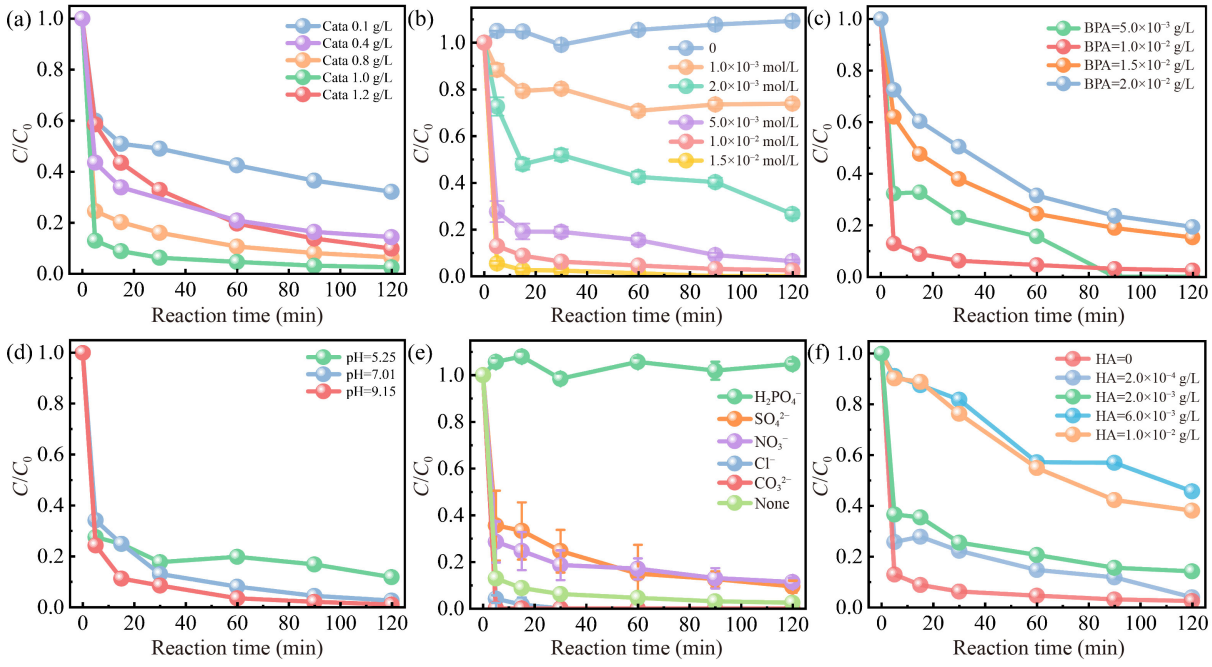

Fig. 4 (a) The catalytic effect of different catalyst dosages for degradation of BPA. (b) The catalytic effect of different H_2O_2 concentrations for degradation of BPA. (c) The catalytic effect of different BPA concentrations. (d) Degradation of BPA in the range pH = 5–9. (e) Influence of different anions (10 mmol/L) in degrading BPA. (f) The catalytic effect of different HA concentrations for degradation of BPA. Reaction conditions: [Catalyst] = 1.0 g/L, [H_2O_2] = 0.01 mol/L, [BPA] = 0.01 g/L, t = 35 °C.

decreased with increasing contaminant concentrations. Nevertheless, 80% of BPA was removed at a contaminant concentration of 20 mg/L. Initial pH was used to evaluate the adaptability of Cu-C-MSNs/H_2O_2 system (Fig. 4(d)). The performance of the catalyst was not significantly affected when the pH ranged between 5.25 and 9.15. Initiating the Fenton reaction in non-acidic environments is typically difficult. However, the degradation of BPA was enhanced under alkaline conditions, which may be attributed to the construction of a polarized electric field that provides additional pathways for contaminant removal. As various salts are usually present in industrial wastewater (Li et al., 2022), investigate the effect of the anions on the activity of the catalyst is necessary (Fig. 4 (e)). In most salt environments, the activity of the Cu-C-MSNs was not significantly affected and the presence of chloride and carbonate salts enhanced the catalyst activity, which was attributed to the hydrolysis of carbonate ions in the solution, established a weakly alkaline environment that promoted contaminant degradation. The effect of HA, a typical DOM, on the activity of the Cu-C-MSNs in simulated natural water was also explored because the complexation of trace ECs with DOM in natural waters can severely hinder ECs removal. The degradation rates of BPA were 96.1% and 85.8% when the HA concentrations were 0.2 and 2 mg/L, respectively (Fig. 4(f)). Cu-C-MSN activity was maintained owing to the construction of cation-π on the catalyst surface, which altered the adsorption sites and degradation pathways of contaminants. However, the performance of Cu-C-MSNs/H_2O_2 weakened when the HA concentrations were 6 and 10 mg/L. Excess HA in solution tended to adsorb and accumulate on the catalyst surface, inhibiting the formation of bond bridges and the electron-donating effect between the Cu sites and contaminants.

The performance of the Cu-C-MSNs for BPA removal under complex conditions demonstrates that the catalyst exhibits excellent activity and strong adaptability in a variety of environments, which has practical significance in wastewater treatment.

3.4 Interfacial reaction mechanism for contaminants degradation

The interfacial electron transfer process and electron supply mechanism of the contaminants in Cu-C-MSNs/H_2O_2 system were revealed by EPR techniques. No $^{\bullet}OH$ signal was detected in the solutions before adding H_2O_2, regardless of the presence of BPA (Fig. 5 (a)). In Cu-C-MSNs/H_2O_2 solution, the signal of $^{\bullet}OH$ was observed with an intensity of 1:2:2:1, implying that H_2O_2 was reduced to $^{\bullet}OH$ by trapping free electrons around the electron-rich Cu sites. The signal intensity of $^{\bullet}OH$ weakened after the addition of BPA to the Cu-C-MSNs/H_2O_2 solution, indicating that $^{\bullet}OH$ was continuously consumed during BPA degradation. In Fig. 5(b), a strong signal of $O_2^{\bullet-}$ was observed in pure Cu-C-MSN

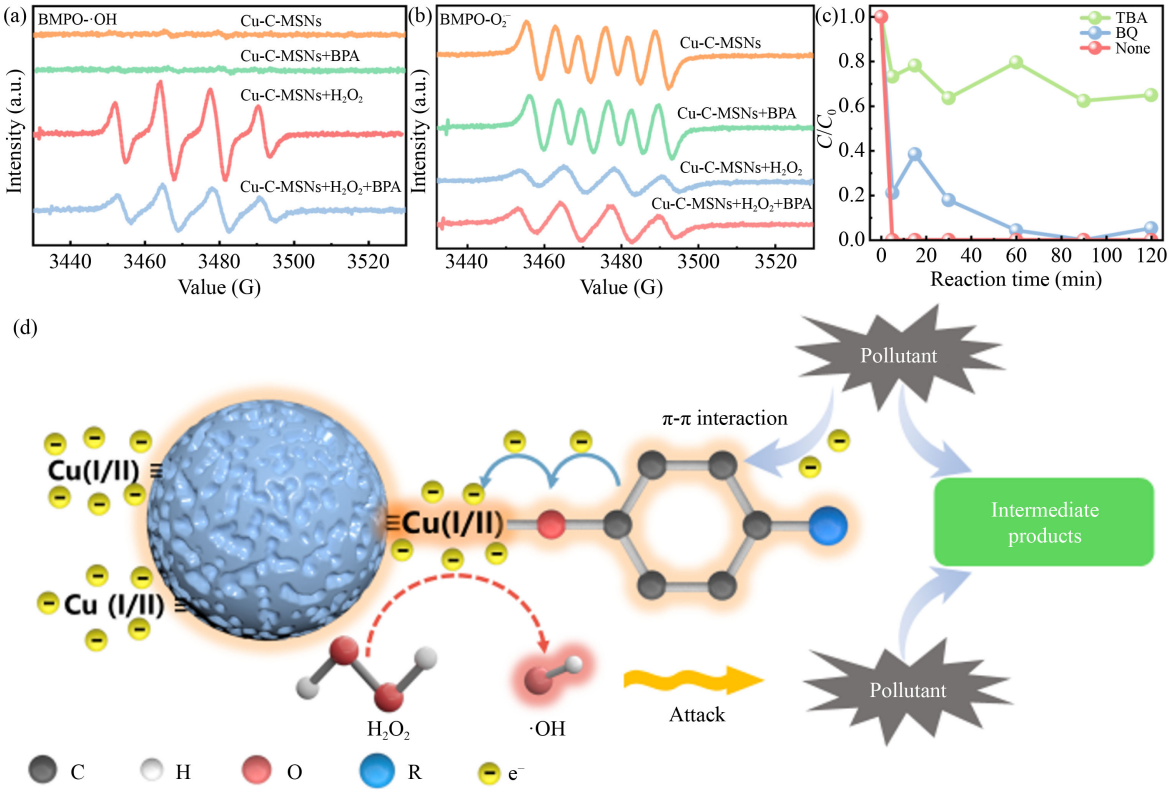

Fig. 5 (a) BMPO trapped •OH in various aqueous. (b) BMPO trapped $O_2^{\bullet-}$ various aqueous. (c) BPA degradation curves in Cu-C-MSNs/H_2O_2 system in the presence of TBA (•OH quenching agent) and BQ ($O_2^{\bullet-}$ quenching agent). (d) Schematic illustration of H_2O_2/O_2 activation and contaminants conversion.

solution, indicating that DO acquired electrons at electron-rich Cu sites and formed $O_2^{\bullet-}$. Nevertheless, the $O_2^{\bullet-}$ signal did not significantly change after the addition of BPA, suggesting that the acquisition of electrons by oxygen simply induced directional transfer of free electrons. Moreover, BPA acts as a new source of electrons to ensure increased electron availability to electron-poor centers through cation-π interaction and π-π interaction. This was verified by analyzing the effects of the anion on the catalyst activity. The dihydrogen-phosphate ion is extremely electronegative and easily occupies electron-poor regions. In the absence of electrons around the Cu center, dihydrogen phosphate is immediately adsorbed onto the electron-poor Cu sites, inhibiting the supply of electrons by BPA. Moreover, no $^1O_2$ was detected in Cu-C-MSNs/H_2O_2 system (Fig. S3). These results were verified by free radical quenching experiments (Fig. 5(c)). The degradation rate of the pollutant decreased by approximately 65% with the addition of •OH quenching agent (TBA), whereas the degradation rate of the pollutant did not change significantly after the addition of $O_2^{\bullet-}$ quenching agent (BQ), suggesting that •OH was the main contributor to the degradation of contaminants.

In conclusion, these results revealed the mechanism behind contaminant degradation by Cu-C-MSNs/ H_2O_2 system (Fig. 5(d)). H_2O_2 acts as an electron acceptor in the electron-rich center (Cu(I)), generating •OH for contaminant degradation. The absence of free electrons and the reduction of L(+)-ascorbic acid led to decreased electron cloud density around Cu(I), which in turn resulted in the conversion of the electron-rich Cu center (Cu(I)) to an electron-poor center (Cu(II)). Contaminants act as electron donors via π–π interactions with graphene-like nanosheets or cation–π interactions (C–O–Cu bond bridges) for the electron-poor center (Cu(II)). The electrons around Si and O are also attracted to and transferred to Cu(II) via the Cu–O–Si bridge for Cu(I)/Cu(II) redox cycling (Zheng et al., 2023). Thus, the contaminants were degraded by the attack of •OH and the surface cleavage in Cu-C-MSNs/H_2O_2 system.

3.5 Intermediates and possible degradation pathways of BPA

The intermediate products of BPA during the reaction were detected using liquid chromatography-mass spectrometry (LC-MS). As shown in Fig. 6(a), 15 intermediates (P1–P15, Table S1), including phenolics, ketones, alcohols, lipids, acids, aldehydes, and quinones, were detected. Based on previous experiments, two degradation pathways for BPA were deduced. In path 1, a

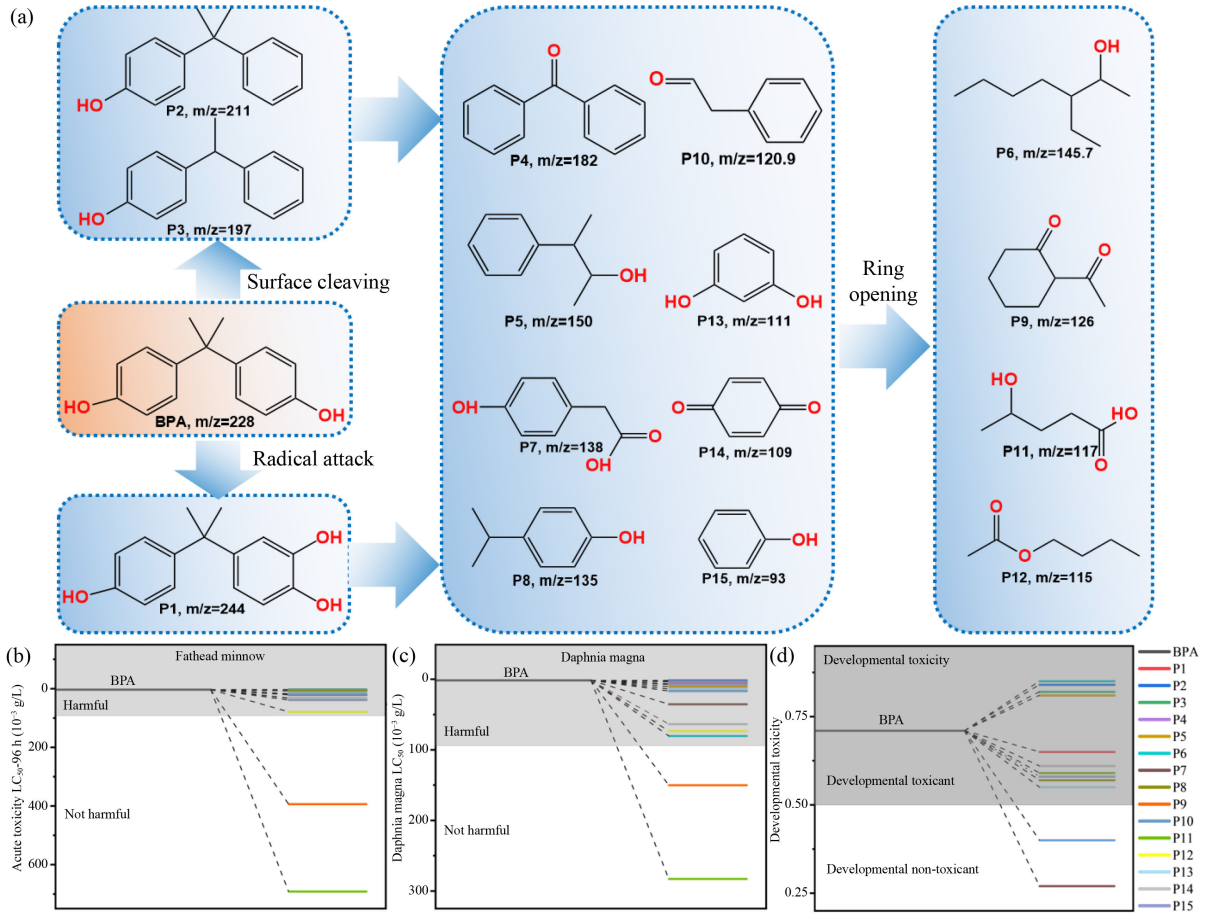

Fig. 6 (a) Proposed degradation pathways in the Cu-C-MSNs system. (b) Fathead minnow LC50 (96 h), (c) Daphnia magna LC50 (48 h), and (d) Developmental toxicity of BPA and its degradation intermediates.

product at m/z = 244 was detected, resulting from the hydroxylation of BPA by an •OH attack. In path 2, BPA was cleaved into 4-(2-phenylpropan-2-yl) phenol and 4-(1-phenylethyl) phenol at m/z = 211 and 197, respectively, after dihydroxylation and demethylation. The aromatic compounds eventually decomposed into lower molecular weight compounds as the reaction continued. Evaluating the toxicity of intermediates during the degradation of contaminants is essential. The fathead minnow LC50 (96 h), *Daphnia magna* LC50 (48 h), and developmental toxicity of BPA and its intermediates were assessed using the Toxicity Estimation Software (T.E.S.T.). The fathead minnow LC50 (96 h) and *Daphnia magna* LC50 (48 h) indicated that BPA was harmful. However, the toxicity of most intermediates was reduced by Cu-C-MSNs/H_2O_2 system, and the intermediates P5 and P7 were also defined as "harmless" (Figs. 6(b) and 6(c)). In addition, the developmental toxicity of most intermediates decreased (Fig. 6(d)). A comprehensive analysis showed that BPA could be degraded to low-toxicity intermediates and be mineralized into H_2O and CO_2.

4 Conclusions

Seaweed spherical microsphere catalysts (Cu-C-MSNs) were successfully fabricated by doping metal species with ascorbic acid into mesoporous silica using an enhanced hydrothermal method. The incorporation of metal species allowed the construction of polarized electric fields, and the addition of ascorbic acid led to the establishment of pathways for contaminants to transfer electrons to the catalysts. These methods allow the catalysts to exhibit outstanding catalytic performance (BPA was degraded by 87% in 5 min), with a wide pH response range and excellent adaptability. Cu-C-MSNs show the ability to purify the actual wastewater, and the biotoxicity of BPA can be reduced by Cu-C-MSNs/H_2O_2. This study revealed different degradation pathways through which •OH attacks ECs; this electron-donating effect leads to the surface cleavage of ECs, providing a new concept for addressing the global environmental crisis.

CRediT Authorship Contribution Statement Yuhang Liu: Design experiments, Methodology Data curation, Formal analysis, Writing original draft. Wenxuan Deng & Xiaojun Wu: Investigation, Performing experiments. Hu Chun & Lai Lyu: Conceptualization, Visualization, Formal

analysis, Writing - review and editing, Supervision, Validation, Resources, Funding acquisition, Project administration.

Acknowledgements This work was financially supported by the National Natural Science Foundation of China (Nos. 52122009, 52070046, and 51838005), the Introduced Innovative R&D Team Project under the "Pearl River Talent Recruitment Program" of Guangdong Province (China) (No. 2019ZT08L387), and the Basic and Applied Basic Research Project of Guangzhou (China) (No. 202201020163).

Declaration of Competing Interests The author Lai Lyu is a Youth Editorial Board Member of *Frontiers of Environmental Science & Engineering*. The authors declare that they have no known competing financial interests or personal relationships that could have appeared to influence the work reported in this paper.

Data Availability Data will be made available on request.

Electronic Supplementary Material Supplementary material is available in the online version of this article at https://doi.org/10.1007/s11783-024-1804-7 and is accessible for authorized users.

References

Alimba C G, Faggio C (2019). Microplastics in the marine environment: current trends in environmental pollution and mechanisms of toxicological profile. Environmental Toxicology and Pharmacology, 68: 61–74

Almeida S, Raposo A, Almeida-González M, Carrascosa C (2018). Bisphenol A: food exposure and impact on human health. Comprehensive Reviews in Food Science and Food Safety, 17(6): 1503–1517

Bing J S, Hu C, Zhang L L (2017). Enhanced mineralization of pharmaceuticals by surface oxidation over mesoporous gamma-Ti-Al_2O_3 suspension with ozone. Applied Catalysis B: Environmental, 202: 118–126

Cao W R, Hu C, Lyu L (2021). Efficient decomposition of organic pollutants over *n*ZVI/FeO_x/FeN_y-Anchored NC Layers via a novel Dual-Reaction-Centers-Based wet air oxidation process under natural conditions. ACS ES&T Engineering, 1(9): 1333–1341

Cuerda-Correa E M, Alexandre-Franco M F, Fernandez-Gonzalez C (2019). Advanced oxidation processes for the removal of antibiotics from water: an overview. Water, 12(1): 102

Do Minh T, Song J, Deb A, Cha L, Srivastava V, Sillanpää M (2020). Biochar based catalysts for the abatement of emerging pollutants: a review. Chemical Engineering Journal, 394: 124856

Gao L H, Cao Y J, Wang L Z, Li S L (2022). A review on sustainable reuse applications of fenton sludge during wastewater treatment. Frontiers of Environmental Science & Engineering, 16(6): 77

Gao T, Lu C, Hu C, Lyu L (2021). H_2O_2 inducing dissolved oxygen activation and electron donation of pollutants over Fe-ZnS quantum dots through surface electron-poor/rich microregion construction for water treatment. Journal of Hazardous Materials, 420: 126579

Gebbie M A, Wei W, Schrader A M, Cristiani T R, Dobbs H A, Idso M, Chmelka B F, Waite J H, Israelachvili J N (2017). Erratum: Tuning underwater adhesion with cation-π interactions. Nature Chemistry, 9(7): 723

Giwa A, Yusuf A, Balogun H A, Sambudi N S, Bilad M R, Adeyemi I, Chakraborty S, Curcio S (2021). Recent advances in advanced oxidation processes for removal of contaminants from water: a comprehensive review. Process Safety and Environmental Protection, 146: 220–256

He X S, Xi B D, Li X, Pan H W, An D, Bai S G, Li D, Cui D Y (2013). Fluorescence excitation-emission matrix spectra coupled with parallel factor and regional integration analysis to characterize organic matter humification. Chemosphere, 93(9): 2208–2215

Hines C J, Christianson A L, Jackson M V, Ye X, Pretty J R, Arnold J E, Calafat A M (2018). An evaluation of the relationship among uurine, air, and hand measures of exposure to bisphenol A (BPA) in US manufacturing workers. Annals of Work Exposures and Health, 62(7): 840–851

Khan M T, Shah I A, Ihsanullah I, Naushad M, Ali S, Shah S H A, Mohammad A W (2021). Hospital wastewater as a source of environmental contamination: an overview of management practices, environmental risks, and treatment processes. Journal of Water Process Engineering, 41: 101990

Khan S, Naushad M, Govarthanan M, Iqbal J, Alfadul S M (2022). Emerging contaminants of high concern for the environment: current trends and future research. Environmental Research, 207: 112609

Li Q Q, Lv C, Xia X W, Peng C, Yang Y, Guo F, Zhang J F (2022). Separation/degradation behavior and mechanism for cationic/anionic dyes by Ag-functionalized Fe_3O_4-PDA core-shell adsorbents. Frontiers of Environmental Science & Engineering, 16(11): 138

López-Suárez F E, Parres-Esclapez S, Bueno-Lopez A, Illan-Gomez M J, Ura B, Trawczynski J (2009). Role of surface and lattice copper species in copper-containing (Mg/Sr)TiO_3 perovskite catalysts for soot combustion. Applied Catalysis B: Environmental, 93(1–2): 82–89

Lu C, Deng K L, Hu C, Lyu L (2020). Dual-reaction-center catalytic process continues Fenton's story. Frontiers of Environmental Science & Engineering, 14(5): 82

Lyu L, Cao W, Yu G, Yan D, Deng K, Lu C, Hu C (2020). Enhanced polarization of electron-poor/rich micro-centers over nZVCu-Cu(II)-rGO for pollutant removal with H_2O_2. Journal of Hazardous Materials, 383: 121182

Lyu L, Hu C (2017). Heterogeneous Fenton catalytic water treatment technology and mechanism. Progress in Chemistry, 29(9): 981–999 (inChinese)

Lyu L, Zhang L, Wang Q, Nie Y, Hu C (2015b). Enhanced Fenton catalytic efficiency of γ-Cu-Al_2O_3 by σ-Cu^{2+}-Ligand complexes from aromatic pollutant degradation. Environmental Science & Technology, 49(14): 8639–8647

Lyu L, Zhang L L, He G Z, He H, Hu C (2017). Selective H_2O_2 conversion to hydroxyl radicals in the electron-rich area of hydroxylated C-g-C_3N_4/ CuCo-Al_2O_3. Journal of Materials Chemistry. A, Materials for Energy and Sustainability, 5(15): 7153–7164

Lyu L, Zhang L L, Hu C (2015a). Enhanced Fenton-like degradation of pharmaceuticals over framework copper species in copper-doped mesoporous silica microspheres. Chemical Engineering Journal, 274: 298–306

Lyu L, Zhang L L, Hu C (2016a). Galvanic-like cells produced by negative charge nonuniformity of lattice oxygen on d-TiCuAl-SiO_2 nanospheres for enhancement of Fenton-catalytic efficiency. Environmental Science. Nano, 3(6): 1483–1492

Lyu L, Zhang L L, Hu C, Yang M (2016b). Enhanced Fenton-catalytic efficiency by highly accessible active sites on dandelion-like copper-aluminum-silica nanospheres for water purification. Journal of Materials Chemistry. A, Materials for Energy and Sustainability, 4(22): 8610–8619

MitićZ, Nikolic G S, Cakic M, Premovic P, Ilic L (2009). FTIR spectroscopic characterization of Cu(II) coordination compounds with exopolysaccharide pullulan and its derivatives. Journal of Molecular Structure, 924–926: 264–273

Morin-Crini N, Lichtfouse E, Liu G R, Balaram V, Ribeiro A R L, Lu Z J, Stock F, Carmona E, Teixeira M R, Picos-Corrales L A, et al. (2022). Worldwide cases of water pollution by emerging contaminants: a review. Environmental Chemistry Letters, 20(4): 2311–2338

Rathi B S, Kumar P S, Show P L (2021). A review on effective removal of emerging contaminants from aquatic systems: current trends and scope for further research. Journal of Hazardous Materials, 409: 124413

Sauvé S, Desrosiers M (2014). A review of what is an emerging contaminant. Chemistry Central Journal, 8(1): 15

Scaria J, Gopinath A, Nidheesh P V (2021). A versatile strategy to eliminate emerging contaminants from the aqueous environment: heterogeneous Fenton process. Journal of Cleaner Production, 278: 124014

Taheran M, Naghdi M, Brar S K, Verma M, Surampalli R Y (2018). Emerging contaminants: here today, there tomorrow. Environmental Nanotechnology, Monitoring & Management, 10: 122–126

Tang F H M, Lenzen M, Mcbratney A, Maggi F (2021). Risk of pesticide pollution at the global scale. Nature Geoscience, 14(4): 206–210

Tran N H, Gin K Y H (2017). Occurrence and removal of pharmaceuticals, hormones, personal care products, and endocrine disrupters in a full-scale water reclamation plant. Science of the Total Environment, 599–600: 1503–1516

Trivedi J, Chhaya U (2022). Bioremediation of bisphenol A found in industrial wastewater using *Trametes versicolor* (TV) laccase nanoemulsion-based bead organogel in packed bed reactor. Water Environment Research, 94(10): e10786

vom Saal F S, Vandenberg L N (2021). Update on the health effects of Bisphenol A: overwhelming evidence of harm. Endocrinology, 162(3): bqaa171

Wang B, Yu G (2022). Emerging contaminant control: from science to action. Frontiers of Environmental Science & Engineering, 16(6): 81

Wang J, Zheng M, Deng Y, Liu M, Chen Y, Gao N, Du E, Chu W, Guo H (2022a). Generality and diversity on the kinetics, toxicity and DFT studies of sulfate radical-induced transformation of BPA and its analogues. Water Research, 219: 118506

Wang X Y, Xu G Z, Tu Y Z, Wu D S, Li A M, Xie X C (2021a). BiOBr/PBCD-B-D dual-function catalyst with oxygen vacancies for Acid Orange 7 removal: evaluation of adsorption-photocatalysis performance and synergy mechanism. Chemical Engineering Journal, 411: 128456

Wang Y, Lyu L, Wang D, Yu H Q, Li T, Gao Y, Li F, Crittenden J C, Zhang L, Hu C (2021b). Cation-Pi induced surface cleavage of organic pollutants with $^{\cdot}OH$ formation from H_2O for water treatment. iScience, 24(8): 102874

Wang Y M, Zhang P, Lyu L, Liao W X, Hu C (2022b). Efficient destruction of humic acid with a self-purification process in an Fe-O-Fe_yC_z/Fe-*x*-GZIF-8-rGO aqueous suspension. Chemical Engineering Journal, 446: 136625

Xiao C, Wang L, Zhou Q, Huang X (2020). Hazards of bisphenol A (BPA) exposure: a systematic review of plant toxicology studies. Journal of Hazardous Materials, 384: 121488

Xing J, Zhang S, Zhang M, Hou J (2022a). A critical review of presence, removal and potential impacts of endocrine disruptors bisphenol A. Comparative Biochemistry and Physiology. Toxicology & Pharmacology: CBP, 254: 109275

Xing X, Li N, Liu D D, Cheng J, Hao Z P (2022b). Effect of Cu-ZSM-5 catalysts with different CuO particle size on selective catalytic oxidation of *N,N*-Dimethylformamide. Frontiers of Environmental Science & Engineering, 16(10): 125

Yamaguchi R, Kurosu S, Suzuki M, Kawase Y (2018). Hydroxyl radical generation by zero-valent iron/Cu (ZVI/Cu) bimetallic catalyst in wastewater treatment: heterogeneous Fenton/Fenton-like reactions by Fenton reagents formed *in-situ* under oxic conditions. Chemical Engineering Journal, 334: 1537–1549

Yazici Guvenc S, Varank G (2021). Degradation of refractory organics in concentrated leachate by the Fenton process: central composite design for process optimization. Frontiers of Environmental Science & Engineering, 15(1): 2

Zhang H, Tang C, Lv Y, Sun C, Gao F, Dong L, Chen Y (2012). Synthesis, characterization, and catalytic performance of copper-containing SBA-15 in the phenol hydroxylation. Journal of Colloid and Interface Science, 380(1): 16–24

Zhang H X, Li C W, Lyu L, Hu C (2020a). Surface oxygen vacancy inducing peroxymonosulfate activation through electron donation of pollutants over cobalt-zinc ferrite for water purification. Applied Catalysis B: Environmental, 270: 118874

Zhang J, Lv B, Xing M, Yang J (2015). Tracking the composition and transformation of humic and fulvic acids during vermicomposting of sewage sludge by elemental analysis and fluorescence excitation-emission matrix. Waste Management, 39: 111–118

Zhang X, Liang J, Sun Y, Zhang F, Li C, Hu C, Lyu L (2020b). Mesoporous reduction state cobalt species-doped silica nanospheres: an efficient Fenton-like catalyst for dual-pathway degradation of organic pollutants. Journal of Colloid and Interface Science, 576: 59–67

Zhao S Y, Chen C X, Ding J, Yang S S, Zang Y N, Ren N Q (2022). One-pot hydrothermal fabrication of $BiVO_4/Fe_3O_4$/rGO composite photocatalyst for the simulated solar light-driven degradation of Rhodamine B. Frontiers of Environmental Science & Engineering, 16(3): 36

Zheng W, You S, Chen Z, Ding B, Huang Y, Ren N, Liu Y (2023). Copper nanowire networks: an effective electrochemical peroxymonosulfate activator toward nitrogenous pollutant abatement. Environmental Science & Technology, 57(27): 10127–10134